uicc
global cancer control

IJC
International Journal of Cancer

A novel ^{19}F agent for detection and quantification of human dendritic cells using magnetic resonance imaging

Fernando Bonetto[1], Mangala Srinivas[1], Arend Heerschap[2], Robbie Mailliard[3], Eric T. Ahrens[4], Carl G. Figdor[1] and I. Jolanda M. de Vries[1]

[1] Department of Tumor Immunology, Nijmegen Centre for Molecular Life Sciences, Radboud University Nijmegen Medical Centre, Nijmegen, Netherlands
[2] Department of Radiology, Radboud University Nijmegen Medical Centre, Nijmegen, Netherlands
[3] Celsense Inc., Pittsburgh, PA
[4] Department of Biological Sciences, Carnegie Mellon University, Pittsburgh, PA

Monitoring of cell therapeutics *in vivo* is of major importance to estimate its efficacy. Here, we present a novel intracellular label for ^{19}F magnetic resonance imaging (MRI)-based cell tracking, which allows for noninvasive, longitudinal cell tracking without the use of radioisotopes. A key advantage of ^{19}F MRI is that it allows for absolute quantification of cell numbers directly from the MRI data. The ^{19}F label was tested in primary human monocyte-derived dendritic cells. These cells took up label effectively, resulting in a labeling of $1.7 \pm 0.1 \times 10^{13}$ ^{19}F atoms per cell, with a viability of 80 ± 6%, without the need for electroporation or transfection agents. This results in a minimum detection sensitivity of about 2,000 cells/voxel at 7 T, comparable with gadolinium-labeled cells. Comparison of the detection sensitivity of cells labeled with ^{19}F, iron oxide and gadolinium over typical tissue background showed that unambiguous detection of the ^{19}F-labeled cells was simpler than with the contrast agents. The effect of the ^{19}F agent on cell function was minimal in the context of cell-based vaccines. From these data, we calculate that detection of 30,000 cells *in vivo* at 3 T with a reasonable signal to noise ratio for ^{19}F images would require less than 30 min with a conventional fast spin echo sequence, given a coil similar to the one used in this study. This is well within acceptable limits for clinical studies, and thus, we conclude that ^{19}F MRI for quantitative cell tracking in a clinical setting has great potential.

Tumor Immunology

Cellular therapy is becoming a key treatment modality for conditions ranging from genetic disorders to cardiovascular disease and cancer.[1–4] Transplanted cells include various types of stem and immune cells for cell-based vaccines. The success of these therapies hinges on the fate of the transplanted cells and on their accurate delivery to target tissues. Hence, it is necessary to monitor the transplanted cells in a noninvasive manner *in vivo*. MRI is often the modality of choice for applications requiring long-term monitoring of transplanted cells because of its noninvasive nature and its nonreliance on short-lived radionuclides.

Dendritic cells (DCs) are the professional antigen-presenting cells of the immune system. Their decisive role in inducing immunity forms the rationale for DC immunotherapy: DCs loaded with relevant antigens are injected into patients to stimulate T cells. DCs have been used extensively in clinical trials[5] aimed at modulating the immune response in cancer, infection, allergy and transplant rejection.[6] DCs may be loaded with relevant antigens before transfer.[7] Alternatively, they can also be loaded with mRNA encoding antigen to aid in antigen presentation *in vivo*.[8,9]

The functionality of DCs is heavily dependent on their location and migratory ability.[10,11] Thus, it is critical to monitor their trafficking *in vivo*. This was first demonstrated in a clinical trial using scintigraphy and MRI to track DCs in melanoma patients, where it was found that the site of transfer of the DCs influenced their trafficking to lymph nodes.[12] This key study was the first example of clinical cell tracking using MRI. However, the difficulty to quantify cell numbers directly from the MRI data using cells labeled with superparamagnetic iron-oxide (SPIO) required the use of scintigraphy. We suggest that the use of ^{19}F MRI for cell tracking would allow both positive localization of the cells and their quantification directly from the image data in a clinical setting.[13] Thus, we tested the labeling of human DCs (as used in

Key words: cell tracking, magnetic resonance imaging, dendritic cell vaccines, cell quantification, perfluorocarbon labels, cellular therapy
Grant sponsors: Netherlands Organization for Scientific Research (NWO, VISTA grant) and by Netherlands Organisation for Health Research and Development (ZonMw); **Grant numbers:** 911-06-021, 917-76-363; **Grant sponsor:** National Institutes of Health; **Grant numbers:** R01-CA134633, R01-EB003453, P01-HD047675, P41-EB001977; **Grant sponsor:** European Commision grant ENCITE; **Grant number:** Health-F5-2008-201842
DOI: 10.1002/ijc.25672
History: Received 5 May 2010; Accepted 17 Aug 2010; Online 13 Sep 2010
Correspondence to: I. Jolanda M. de Vries, Department of Tumor Immunology, Radboud University Nijmegen Medical Center, P.O. Box 9101, 6500 HB Nijmegen, Netherlands, Tel.: 31-3617600, Fax: 31-24-3540339, E-mail: j.devries@ncmls.ru.nl

cancer vaccine trials) with a clinically applicable, commercial ^{19}F agent. This technique has not yet been applied to clinical cell tracking, and this article explores the feasibility of clinical ^{19}F MRI in this setting.

The labels used for MRI-based cell tracking fall into two broad categories, namely contrast agents and tracer agents containing nuclear magnetic resonance active nuclei other than ^{1}H. Contrast agents result in localized changes of intensity in the ^{1}H image. Specifically, iron-based agents such as SPIO often result in a drop in apparent spin–spin relaxation time T_2^* around the agents and thus a region of hypointensity in the ^{1}H image. DCs have been tracked using SPIOs in melanoma patients.[12] Other metal-based agents, such as Gadolinium (Gd), cause a decrease in the spin-lattice relaxation time T_1 and thus a localized region of hyperintensity in T_1-weighted images.[14] For all contrast agents, the large ^{1}H background hampers accurate quantification.[15] The use of a second nucleus for imaging is a relatively new paradigm in MR-based cell tracking.[16–18] The relevant nucleus is imaged and a ^{1}H image is obtained separately solely for anatomic information. ^{19}F has been the main focus due to its sensitivity, which is comparable to that of the ^{1}H nucleus. Moreover, the negligible endogenous concentration of ^{19}F *in vivo* leads to a complete absence of background in ^{19}F images, simplifying positive identification of the label and, therefore, also relatively simple quantification of label within a voxel.[18] Indeed, ^{19}F imaging has been developed as an *in vivo* cytometry assay.[19]

Here, we demonstrate the utility of a novel, potentially clinically applicable ^{19}F agent, CS-1000 (Celsense Inc., USA) for cell tracking and quantification directly from image data, in comparison to conventional metal-based contrast agents, applied to primary human DCs as used in current cancer vaccine trials.

Material and Methods

DC purification and labeling

DCs were generated from adherent peripheral blood mononuclear cells, from donor blood, by culturing in the presence of interleukin-4 (500 U/ml) and granulocyte-monocyte colony stimulating factor (800 U/ml) (both Cellgenix, Freiburg, Germany). Cells were cultured in X-VIVO 15 medium (BioWhittaker, Walkersville, MD) with 2% human serum (Bloodbank; Rivierenland, Nijmegen, The Netherlands)[20] at a concentration of 5×10^5 cells per ml of medium. Label consisting of either CS-1000 (Celsense, USA) at the indicated concentrations, 200 μg ferumoxide/ml of Endorem (Gueberet, France) or 1 mM ProHance (Bracco, Italy) was added on Day 3. CS-1000 is an aqueous colloidal nanoemulsion of a perfluorocarbon polymer. The total fluorine content is 100 mg/ml, and the droplet size of the nanoemulsion is 180 nm. It is specifically formulated to facilitate internalization of the reagent into any cell type *ex vivo*, regardless of inherent phagocytic ability. The perfluorocarbon molecule used is stable at low pH, lipophobic and hydrophobic, and is not degraded by any cell enzymes.[21] At Day 6, DCs were matured by the addition of 10 μg/ml PGE_2 (Pharmacia & Upjohn, Puurs, Belgium), 10 ng/ml TNF-α, 5 ng/ml IL-1β and 15 ng/ml IL-6 (Cellgenix). On Day 8, the cells were harvested and washed using cold phosphate buffered saline solution to remove excess label. Cell viability was determined by trypan blue exclusion.

Electroporation was done as described elsewhere.[8] Briefly, 20 μg of RNA was transferred to a 4 mm cuvette (BioRad, Veenendaal, The Netherlands), and 10 million cells are added over it in 200 μl OptiMEM without phenol red (Invitrogen, Breda, The Netherlands). After a 3 min incubation, the sample was pulsed in a Genepulser Xcell (BioRad) at 300 V and 150F with an exponential decay pulse. After electroporation, cells were transferred to prewarmed X-VIVO 15 without phenol red (Cambrex Bio Science, Verviers, Belgium) with 5% human serum and incubated for 3 hr at 37°C.

MR imaging and MR spectroscopy

In vitro measurements. ^{1}H and ^{19}F MRI for *in vitro* samples were performed on a 7 T horizontal bore MR system (Surrey Medical Imaging Systems, United Kingdom) with a 10-mm-diameter ^{1}H/^{19}F double-tuned single surface coil. ^{1}H images were acquired by using T_1-weighted spin echo and T_2^*-weighted gradient echo pulse sequences with a repetition time (TR)/echo time (TE) = 1000/4 msec and TR/TE = 2000/15 msec, respectively, resolution $0.125 \times 0.125 \times 2$, matrix size 128×128, 4 averages. ^{19}F spin density-weighted images were acquired using a spin echo sequence with TR/TE = 300/4 msec, resolution: $1 \times 1 \times 2$ mm, matrix size: 16×16 mm, 1024 averages. ^{19}F T_1 and T_2 values for the fluorinated label were measured to be 350 ± 20 msec and 44 ± 8 msec, respectively, at 7 T, when internalized into the cells. ^{1}H T_1 and T_2^* relaxation times for different Gd and SPIO-labeled cell concentrations were measured using the inversion recovery pulse sequence and determining the minimum full width at half maximum of the spectrum at the best shimming conditions, respectively. MR Spectroscopy was used to determine ^{19}F content per cell with a calibrated reference of triflouroacetic acid (TFA) by applying an adiabatic 90° pulse to excite the whole sample.

For MRI, a variable number of labeled DCs were embedded in gelatin. Alternatively, 1.5 million labeled cells were injected into bovine muscle tissue and imaged. Relative T_1 and T_2^* were referred to the values of a reference sample consisting of gelatin with nonlabeled cells, and to the TFA reference for ^{19}F images.

In vivo measurements. *In vivo* MR images were acquired at 11.7 T using a 89 mm vertical-bore Bruker microimaging system (Bruker Biospin, Billerica, MA) equipped with a 35-mm-diameter volume coil that can tune between 470 and 500 MHz for ^{19}F and ^{1}H, respectively. ^{19}F-labeled human DCs ($\sim 3 \times 10^6$) were injected subcutaneously into a quadriceps of a female NOD-SCID mouse, 6 weeks of age. The mouse was anesthetized (1.5% isoflurane in 80% O_2 and 20% N_2O),

intubated and placed on a mechanical ventilator with respiratory gating. Body temperature was maintained at 37°C. ^{19}F images were acquired by using a rapid acquisition with relaxation enhancement (RARE) sequence with TR/TE = 500/11.5 msec, RARE factor 8, 64 × 64 image points, 45 × 30 mm in-plane field of view, 2 mm slice thickness, and 256 averages; and ^{1}H images using a spin-echo sequence with TR/TE = 100/15, 4 averages, 256 × 256 image points, and the same field of view and slice thickness as the ^{19}F. Experiments were carried out in accordance with the guidelines provided by the Carnegie Mellon Institutional Animal Care and Use Committee (IACUC) and the National Institute of Health Guide for the Care and Use of Laboratory Animals.

MRI-based quantification

The "relative intensity" for the ^{1}H data (Fig. 3*b*) was calculated using the relation $\left|\frac{I_{\text{cell}}-I_{\text{control}}}{I_{\text{control}}}\right| \times 100\ \%$, where I_{cells} is the total signal intensity over the labeled cells. I_{control} is the total signal intensity over a region of similar size containing nonlabeled cells. In all cases, intensity was summed for all voxels in-plane. Note that $I_{\text{cells}} - I_{\text{control}}$ is the change in signal intensity due to the labeled cells.

To calculate the signal-to-noise ratio (SNR) of ^{19}F MR images, the noise magnitude N was first determined by averaging the intensity of the voxels near the border of the image. Next, voxels with ^{19}F signal intensity higher than $3N$ were selected, and the signal intensity of each voxel was corrected to account for the Rician-distributed noise present in intensity images with low SNR.[22] The threshold for detection was fixed at SNR = 3.

To perform the cell density map calculation (Fig. 4*b*), the signal intensity values for each voxel and for every slice with SNR > 3 were determined as explained above. The total signal intensity (sum of all signal intensities from all voxels over all slices) was then calculated and associated with the total amount of cells injected into the tissue. Finally, the number of cells in each voxel was calculated by normalizing the signal obtained against the total signal intensity. The density of cells for each voxel was calculated by considering the voxel volume. All errors shown are the standard deviation.

Flow cytometry

Fluorescence activated cell sorter (FACS) analysis was performed using with a FACSCalibur™ flow cytometer equipped with CellQuest software (BD Biosciences, Mountain View, CA). The primary antibodies used were anti-CD80 (BD Biosciences), anti-CD83 (both Beckman Coulter, Mijdrecht, The Netherlands), anti-CD86 and anti-CCR7 (both BD PharMingen, San Diego, CA). Secondary staining was with isotype appropriate goat-anti-mouse Alexa648 (Invitrogen). Intracellular staining for mRNA expression was carried out on cells permeabilized in PBS with 2% bovine serum albumin (BSA), 0.02% azide and 0.5% saponin (Sigma-Aldrich) (PBA/saponin), and stained with mAb diluted in PBA/saponin with 2% HS, followed by staining with allophycocyanin-labeled goat-anti-mouse (BD PharMingen).

Results

^{19}F labeling of primary human DCs

We studied the labeling of human DCs with the ^{19}F CS-1000 agent. Cells were incubated with CS-1000 under various conditions. DCs take up CS-1000 effectively, without a need for transfection aids (Fig. 1*a*). Label was added to immature DCs, and the cells were incubated for 3 days before the addition of maturation factors. Significant toxicity was observed only at high concentrations of label (Fig. 1*a*). Uptake appears to saturate at 140 μl of label per million of cells. Based on these data, we used 75 μl of CS-1000 per million cells on Day 3 after starting the monocyte culture, *i.e.*, with immature DCs, for all further experiments. Note that these cells do not undergo cell division. This yielded 1.7 ± 0.1 × 10^{13} ^{19}F atoms per cell, with an acceptable viability of 80 ± 6%. The low standard deviation of ^{19}F content/cell obtained after measuring three independent samples also suggests homogeneous cell labeling.

^{19}F labeling has minimal effect on primary human DCs

The DCs were analyzed after labeling, to study any possible effect of CS-1000 on the cells. General visual inspection under the microscope showed no difference with nonlabeled controls, except for the bigger size and the presence of label droplets in the labeled cells. Consistent with this observation, a difference in side scatter between labeled and nonlabeled DCs was clearly seen (Fig. 1*b*) because of the presence of intracellular label droplets. The expression of the DC maturation markers CD80, CD86, CD83 and CCR7 was unchanged in labeled cells relative to untreated controls (Fig. 1*c*, left). Furthermore, the label had no effect on protein expression after mRNA electroporation (Fig. 1*c*, right), which is a typical step in clinical DC vaccination trials.[8] A mixed leukocyte reaction using labeled and nonlabeled DCs to stimulate allogeneic lymphocytes showed no difference in T cell activation between the two groups at all DC:lymphocyte ratios tested (p = 0.05; data not shown). From all these data, we conclude that CS-1000 has no negative effects on DC viability, antigen expression and maturation.

Detection sensitivity

Standard imaging sequences were used in our studies, as outlined in Materials and Methods. Cells were resuspended at known densities in gelatin for determination of the minimum number of cells per voxel necessary for detection (Fig. 2*a*). We found the minimum detectable density of ^{19}F-labeled cells to be comparable with that of Gd-labeled cells when assessed visually, at under 2000 cells/voxel when imaged with a ^{19}F spin density weighted and ^{1}H T_1-weighted sequence, respectively. The detection limit using SPIO was lower, ∼125 cells/voxel, using T_2^*-weighted imaging in our system (Fig. 2*b*). However, these data were acquired with a homogenous

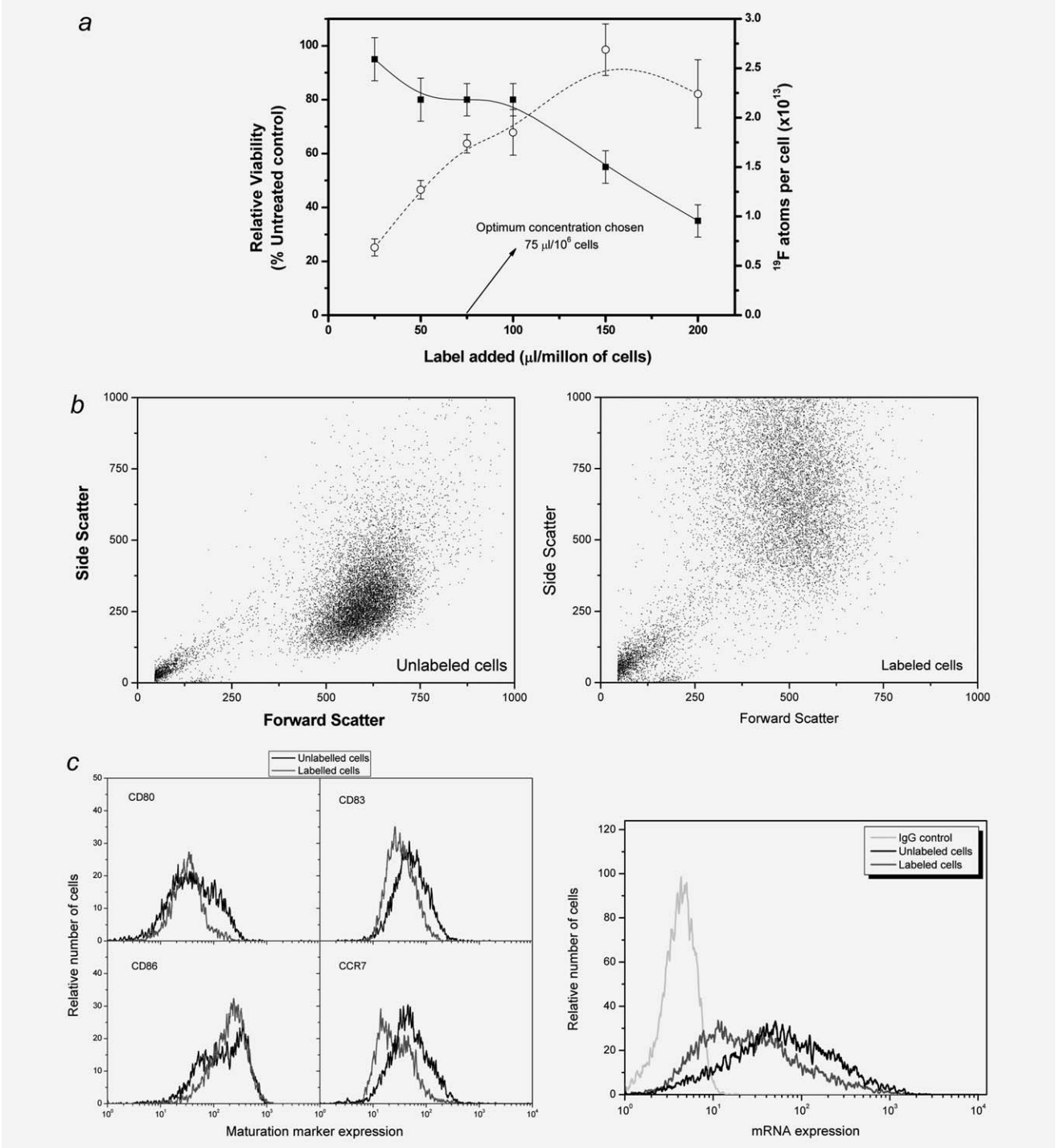

Figure 1. Labeling primary human DCs with ^{19}F has minimal effect on cell functionality. Cells were labeled with CS-1000 by coincubation, at the concentrations indicated. They were then washed and processed for MRS or other assays. (*a*) ^{19}F uptake (open circles, right *y*-axis) was measured using MRS on cell pellets with a calibrated reference. Viability after labeling (full squares, left *y*-axis) was measured using a trypan blue exclusion assay. We observed toxicity only at high label concentrations. The optimum selected concentration is indicated in the figure. (*b*) Flow cytometric analysis on the untreated controls (left) shows a clear difference in side scatter relative to labeled cells (right). Gating was on live cells. (*c*) The plot on the left shows no change in expression of standard DC markers after labeling (grey) relative to untreated cells (black). Cells were labeled and then electroporated with tumor-derived mRNA (right). Protein expression was analyzed using intracellular staining for flow cytometry and plotted in the histogram. ^{19}F labeling did not affect mRNA uptake relative to nonlabeled controls.

^{1}H background and are not directly comparable to *in vivo* sensitivity.

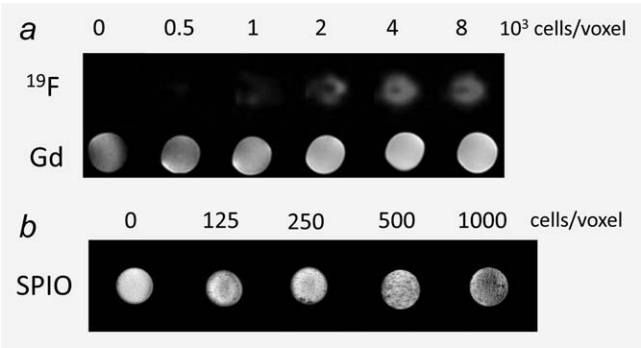

Figure 2. MR images of labeled cells in phantoms with increasing cell densities. Cells were labeled with ^{19}F, Gd or SPIO and suspended in gelatin at various cell densities. Axial slices were then acquired. (*a*) The panel shows MR images for ^{19}F and Gd-labeled cells at 500–8,000 cells/voxel. Images of the Gd-labeled cells were normalized to a reference consisting of nonlabeled cells in gelatin. (*b*) T_2^*-weighted axial images of cells labeled with SPIO at 0–1000 cells/voxel in phantoms.

Cell number quantification

The number of labeled DCs in a region of interest was evaluated from the MR image data. Cells were labeled with Gd, SPIO or ^{19}F and suspended at various, known densities in gelatin for imaging, as before. Figure 3*a* shows the linear relationship between ^{19}F intensity and the number of cells per voxel. A similar linear relationship exists between the SNR and cell density. Thus, the cell number can be calculated directly from image data, if the label content per cell is known.

The plots for Gd and SPIO-labeled cells (Fig. 3*b*, left and right, respectively) show the more complex relationship between T_1, T_2^* and relative contrast in the image. The change in contrast begins to saturate at about 8,000 cells/voxel with Gd and as early as with 800 cells/voxel using SPIO. These issues complicate cell number quantification using contrast agents but not ^{19}F labels.

Cell localization over tissue background

DCs (1.5 million) were labeled either with SPIO, Gd or ^{19}F and injected as a bolus in bovine muscle tissue and imaged to study detection sensitivity over tissue background. The corresponding images are shown in Figure 4*a*. Unlabeled cells were also injected similarly as a negative control. This control

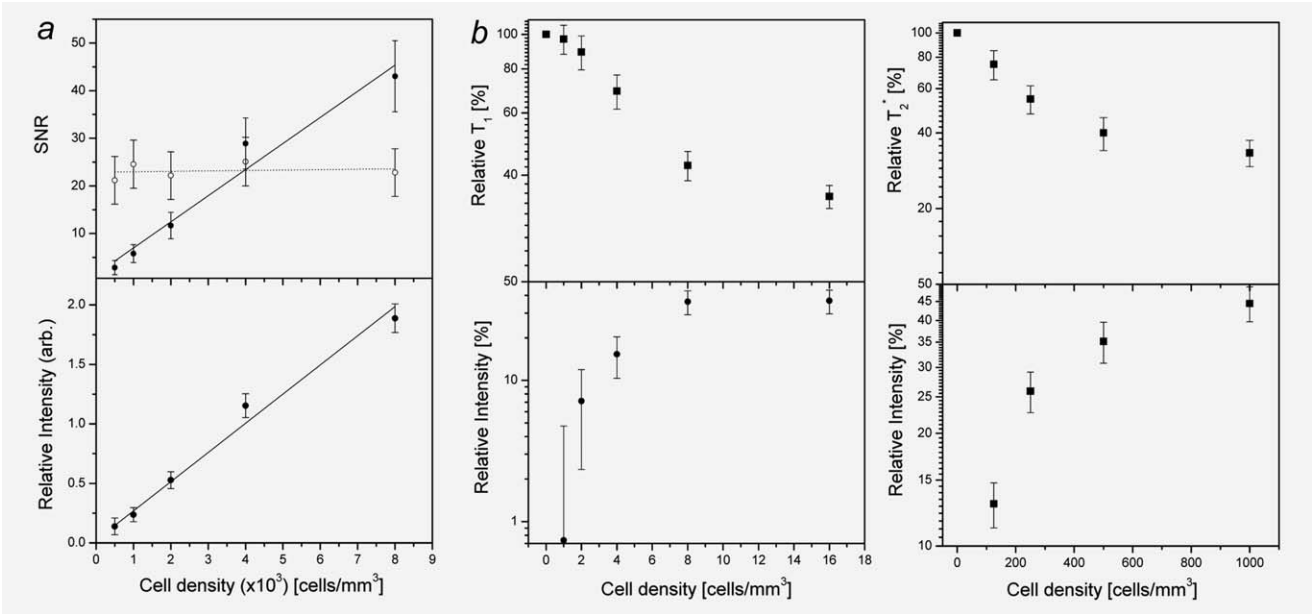

Figure 3. Cell quantification from MR images data. Cells were labeled, suspended at various densities in gelatin and imaged using the appropriate spin-density, T_1 or T_2^*-weighted sequence. (*a*) The signal intensity of the labeled cells relative to a calibrated ^{19}F reference with constant ^{19}F content was calculated and plotted, showing the linear relationship between cell density and signal intensity. The plots show the SNR (upper panel) and signal intensity relative to the reference (lower panel) for the ^{19}F-labeled cells and ^{19}F reference (closed and open circles respectively). Relative intensity here is the ratio between the SNR of the labeled cells (full circles in the upper panel) and SNR of the reference sample (open circles in the upper panel). (*b*) Similar data were plotted for cells labeled with Gd and SPIO. Cells labeled with Gd (left) were imaged using a T_1-weighted scan, and the relative signal intensity (lower panel) and T_1 plotted with increasing cell density (upper panel). Relative intensity is the change in contrast due to the presence of label. Similar plots for SPIO-labeled cells (right) show the relative T_2^* (upper panel) and intensity (lower panel). All values for the Gd and SPIO cells are normalized to the relaxation parameters and signal intensity over a reference containing nonlabeled cells. All plots in Figure 3*b* are presented in a logarithmic scale. The observed depart from the linear behavior is clearly showing the difficulties of quantification process when contrast agents are used.

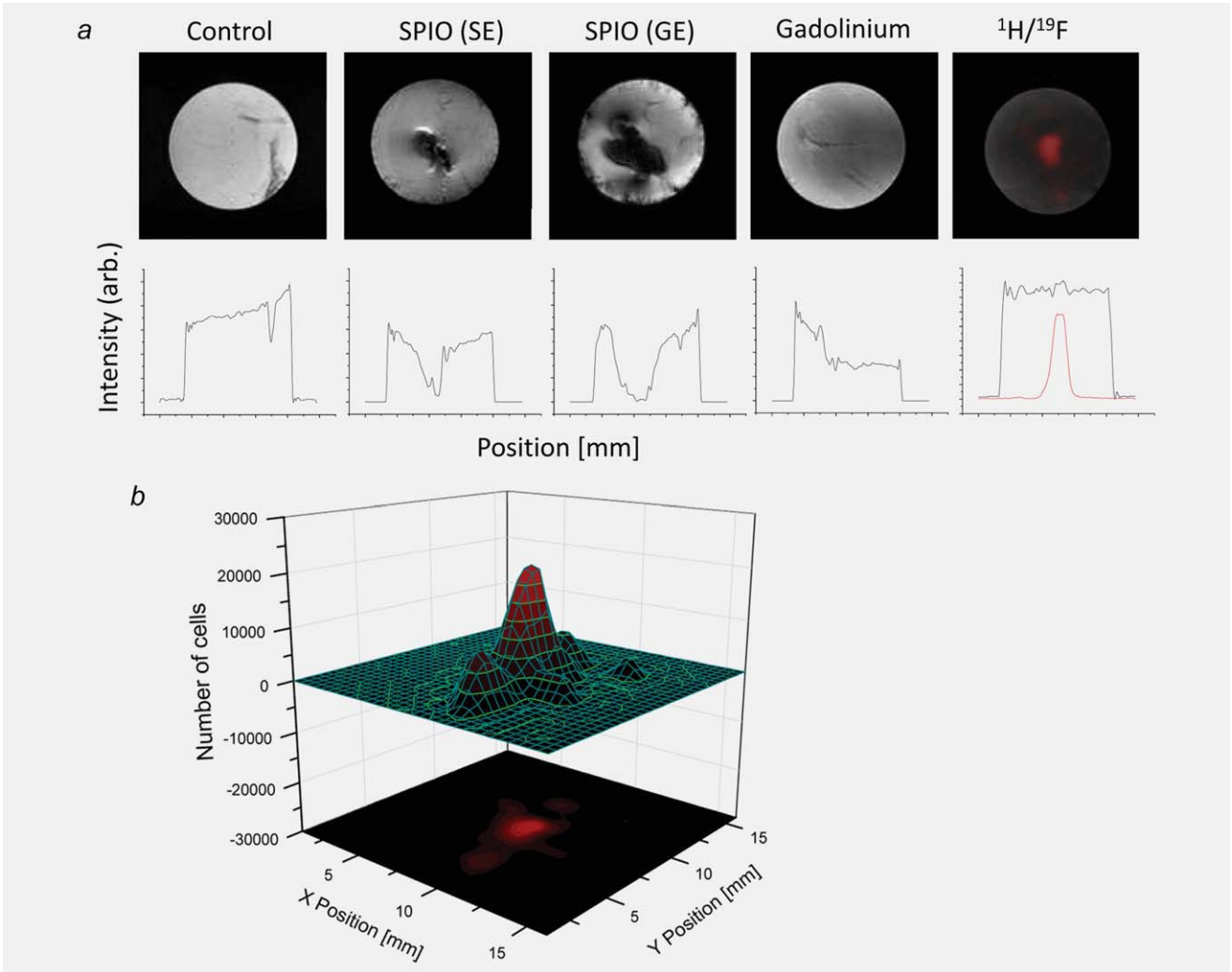

Figure 4. Detection and identification of labeled DCs in muscle tissue. 1.5 million cells were labeled with SPIO, Gd or ^{19}F (false color) and injected as a bolus in bovine muscle tissue. (*a*) Unlabeled cells were used as a control, which shows the typical nonhomogenous ^{1}H background of tissue. The cells labeled with SPIO were imaged with both an spin-echo (SE) and a gradient-echo (GE) sequence. ^{19}F-labeled cells are clearly visible (false color). The lower panels show the corresponding intensity profiles for a horizontal line through center of the sample, showing the intensity of the pixels at a given position. All plots are set to the same scale. (*b*) A cell number map of the ^{19}F-labeled cells in the slice was calculated from the image data. A projection of the calculated slice is shown, which corresponds with the original ^{19}F image.

shows the typical nonhomogeneous background from biological tissue, unlike with gelatin phantoms (Fig. 2). The contrast due to SPIO is apparent in the bolus injection, but the Gd-labeled cells are not readily detected in this image over the background. The ^{19}F-labeled cells are clearly visible and readily differentiated against the ^{1}H tissue underlay (Fig. 4*a*). The plots under the corresponding images show the signal intensity through a horizontal line across the center of the sample (plotted in red for the ^{19}F image), where all are set to the same scale. As expected, the SPIO-labeled cells display a sharp drop in signal intensity, and the Gd-labeled cells show a slight peak in its intensity profile. The ^{19}F-labeled cells are readily identified, even though the SNR of the ^{19}F data is lower than that of the ^{1}H images.

The cell density in the slice containing the ^{19}F-labeled cells was calculated from the image data and is shown in Figure 4*b*. As expected for a bolus injection, the highest cell density was at the center of the injection site. These findings demonstrate the relative ease of quantification using ^{19}F agents. As it can be inferred from Figure 4*b*, the sensitivity obtained was again in the order of 2,000 cells/voxel, affirming that sensitivity and quality of ^{19}F images are not affected by the presence of tissue background.

To demonstrate the feasibility of *in vivo* ^{19}F tracking, 3×10^6 mature, labeled human DCs were injected and imaged in mouse. Figure 5 displays the fused ^{1}H and ^{19}F image 12 hr postinjection. Labeled cells are clearly visible in the ^{19}F image, localized in a region anatomically consistent with the

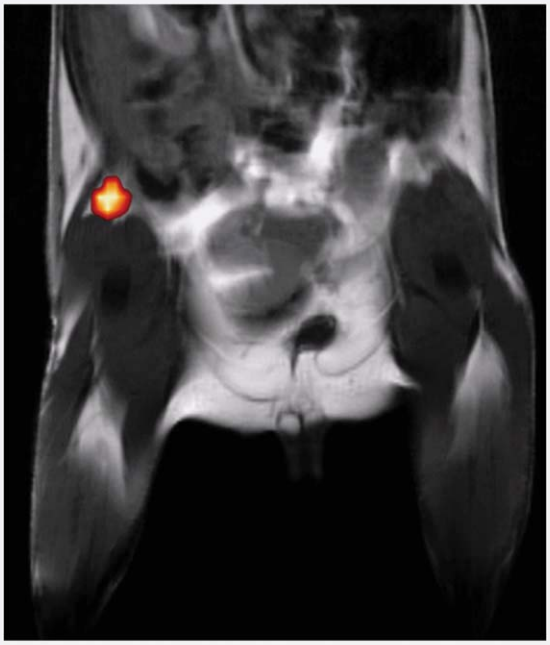

Figure 5. *In vivo* detection of labeled human DCs in a xenograft mouse model. CS-1000 labeled DCs were injected subcutaneously in an NOD-SCID mouse. Shown is fused $^{19}F/^{1}H$ image, where the ^{19}F is rendered in false color and the ^{1}H is in grayscale. The DCs are visible as a "hot spot" in an anatomical location consistent with the draining inguinal lymph node on the side of the cell injection.

proximal draining inguinal lymph node. As the cells were subcutaneously injected in the quadriceps, this image shows cell migration away from the injection site.

This image also demonstrates that 3×10^6 cells can easily be visualized *in vivo* at 11.7T with a measurement time of 28 min. The absence of any ^{19}F background signal indicates that the presence of isoflurane is under detection limits and it can be neglected in this experiment. However, an alternative non-fluorinated anesthetic should be used when lower cell densities need to be measured or with longer scan times.

Discussion

We show that a commercially available perfluorocarbon emulsion is a promising label for ^{19}F MRI-based cell tracking in a clinically relevant cell type. We found that the CS-1000 label had minimal effect on DC viability and function, as tested by expression of maturation markers, mRNA expression after electroporation and T cell activation. The minimum number of labeled cells per voxel detectable at 7T with our imaging parameters is ~2000, with 1.7×10^{13} fluorine atoms per cell. This labeling is consistent with previously published data using similar ^{19}F labels in murine cells.[18,23] Uptake of label by mature DCs was much lower (data not shown) as maturation downregulates endocytic processes; hence, we labeled the cells in the immature stage. Labeling was observed within 24 hr after addition of label, although we cultured the cells for 6 days after label addition to minimize cell handling steps.

The detection limit using SPIO *in vitro* is almost 10-fold lower than either the ^{19}F or the Gd labels (Figs. 2 and 3). This is comparable with previous reports on the sensitivity of MRI for the detection of human DCs labeled with SPIO at 1,000 cells/mm^3 *in vitro* when loaded with 30 pg Fe/cell.[24] SPIO agents can be extremely sensitive, and detection limits as low as single cells have been reported using SPIO agents *in vitro*.[25–27] However, the addition of ^{1}H background from biological tissue complicates identification of labeled cells (Fig. 4*a*), as endogenous regions of hypointensity are observed in various tissues, blood vessels or blood clots. In addition, the T_1 and T_2^* effects are not independent of each other. Most importantly, the effect of contrast agents on relaxivity saturates at higher concentrations (Fig. 3*b*). T_2^* agents are particularly sensitive to this saturation effect (Fig. 3).

Cell number quantification using T_2^* agents is prone to error due to the uncertainty in agent relaxivity *in situ* and at higher cell densities due to the saturation of the T_2^* effect, as demonstrated in Figure 3*b*. Cheung *et al.* carried out quantification of cells in phantoms using a ultrasmall SPIO agent and found that the cell numbers were underestimated at cell densities greater than approximately one million cells per voxel.[28] This may be a limitation of the technique given that the typical cell numbers injected in a clinical DC vaccination trial is about 15 million[12] and cell numbers can be even higher with other cell therapies. Other techniques to decipher the complex change in observed contrast with SPIO labels involving quantitative measures of relaxation rates are also susceptible to the same saturation effect.[15] Recent advances with contrast agents include the use of "white markers" for cell localization using T_2^* agents.[15,28–31] In this technique, the background is made dark by dephasing gradients, and the intensity of the signal near the contrast agent dipoles is dependent on relaxivity, echo-time, slice thickness and gradient strength.[30] Endogenous iron stores and blood clots at the site of injection also complicate relaxometric measurements at the site of cell transfer.[32]

It is also worth to mention that as we used monocytes-derived DCs, these cells do not divide.[32] This fact makes the method used for cell quantification particularly suitable for tracking DCs since no signal reduction nor data misinterpretation are caused by the uncontrolled process of cell division. However, the technique of quantitative cell tracking using ^{19}F MRI has also been applied to actively dividing T cells, which were successfully tracked for up to 3 weeks.[32] The underestimation of cell numbers that occurs due to cell division is often within tolerable limits, two–fourfold depending on the division rate and length of time. This error can be reduced if the cell division rate is known. Exocytosis of the label after cell death could also be a source of error in the quantification method, but only relevant when the number of dead cells is in the same order of magnitude

as living cells. This issue is discussed in more detail elsewhere.[13]

Together, our findings demonstrate the feasibility of ^{19}F labeling of human DCs and cell quantification using MRI. The label shows comparable detection sensitivity to cells labeled *in vitro* using Gd-complexes when imaged using conventional contrast mechanisms. The main limitation of ^{19}F imaging is the low concentration that necessitates the use of signal averaging and potentially longer scan times. Our current detection limit of 2,000 cells/voxel at 7T with $1.7 \pm 0.1 \times 10^{13}$ ^{19}F atoms/cell translates to a limit of about 9,000 cells/voxel at 3T (considering a strong $SNR \infty B_o^{7/4}$ dependence with the magnetic field intensity B_o for small coils), with other factors remaining constant. To put this into perspective, a typical DC vaccination study utilizes an intranodal or intradermal injection of about 10 million cells, with between 30,000 and 200,000 cells migrating to secondary lymph nodes, as detected using scintigraphy on ^{111}In-labeled DCs.[33] We note that the size of a voxel in MRI is determined by the practitioner, and high resolution imaging is not necessary for ^{19}F-based cell localization as these images are overlaid onto high resolution ^{1}H images for anatomy. Importantly, the SNR needed for ^{19}F images can generally be much lower (*e.g.*, SNR5 or less) than normally acceptable for ^{1}H images, as the ^{19}F is not used to provide tissue contrast or organ definition, but only cell population localization. Moreover, further improvements in ^{19}F MRI methodologies might yield significant imaging acceleration, for example using restricted *k*-space acquisitions schemes.[34]

Currently, clinical ^{19}F MRS requires a concentration of ^{19}F in the millimolar range.[35,36] Our current detection limits of 2,000 or 9,000 cells/voxel at 7 T and 3 T, respectively, translate to concentrations of ^{19}F at 1 and 5 mM. The clinical MR spectroscopy work suggests that these concentrations can be achieved and detected using human scanners.

Thus, to image a lymph node with 30,000–200,000 cells based on our system (acquired using the same coil) would take 30–0.7 min at 3T, while maintaining a minimum SNR of 3 for ^{19}F (sufficient for quantification[18,19]) when using a single spin echo sequence. The use of a fast multiecho imaging sequence,[18,19] typical in clinical applications, with a turbo factor (RARE factor) of 4 would result in imaging times of 8–0.2 min for 30,000–200,000 cells, which are within reasonable limits for clinical use. Overall, realistic advances in hardware and imaging protocols may allow *in vivo* ^{19}F-based cell tracking to become clinically relevant in the near future.

Acknowledgements

The authors would like to specially thank Andor Veltien for the ^{19}F/^{1}H coil construction and very helpful discussions. They also acknowledge to Mandy van de Rakt, Nicole Meeusen-Scharenborg, Annemiek de Boer, Dr. Gerty Schreibelt, Dr. Annechien Lambeck and Mark van Uden.

References

1. Akins EJ, Dubey P. Noninvasive imaging of cell-mediated therapy for treatment of cancer. *J Nucl Med* 2008;49 Suppl 2: 180S–95S.
2. Bhagavati S. Stem cell based therapy for skeletal muscle diseases. *Curr Stem Cell Res Ther* 2008;3:219–28.
3. Roh JK, Jung KH, Chu K. Adult stem cell transplantation in stroke: its limitations and prospects. *Curr Stem Cell Res Ther* 2008;3:185–96.
4. Yamahara K, Nagaya N. Stem cell implantation for myocardial disorders. *Curr Drug Deliv* 2008;5:224–9.
5. Aarntzen EH, Figdor CG, Adema GJ, Punt CJ, de Vries IJ. Dendritic cell vaccination and immune monitoring. *Cancer Immunol Immun* 2008;57:1559–68.
6. Steinman RM, Banchereau J. Taking dendritic cells into medicine. *Nature* 2007; 449:419–26.
7. Lesterhuis WJ, de Vries IJ, Adema GJ, Punt CJ. Dendritic cell-based vaccines in cancer immunotherapy: an update on clinical and immunological results. *Ann Oncol* 2004;15 Suppl 4:iv145–51.
8. Schuurhuis DH, Lesterhuis WJ, Kramer M, Looman MG, van Hout-Kuijer M, Schreibelt G, Boullart AC, Aarntzen EH, Benitez-Ribas D, Figdor CG, Punt CJ, de Vries IJ, et al. Polyinosinic polycytidylic acid prevents efficient antigen expression after mRNA electroporation of clinical grade dendritic cells. *Cancer Immunol Immunother* 2008;58:1109–15.
9. Schuurhuis DH, Verdijk P, Schreibelt G, Aarntzen EH, Scharenborg N, de Boer A, van de Rakt MW, Kerkhoff M, Gerritsen MJ, Eijckeler F, Bonenkamp JJ, Blokx W, et al. In situ expression of tumor antigens by messenger RNA-electroporated dendritic cells in lymph nodes of melanoma patients. *Cancer Res* 2009;69: 2927–34.
10. Verdijk P, Aarntzen EH, Lesterhuis WJ, Boullart AC, Kok E, van Rossum MM, Strijk S, Eijckeler F, Bonenkamp JJ, Jacobs JF, Blokx W, Vankrieken JH, et al. Limited amounts of dendritic cells migrate into the T-cell area of lymph nodes but have high immune activating potential in melanoma patients. *Clin Cancer Res* 2009; 15:2531–40.
11. Verdijk P, Aarntzen EH, Punt CJ, de Vries IJ, Figdor CG. Maximizing dendritic cell migration in cancer immunotherapy. *Expert Opin Biol Ther* 2008;8: 865–74.
12. de Vries IJ, Lesterhuis WJ, Barentsz JO, Verdijk P, van Krieken JH, Boerman OC, Oyen WJ, Bonenkamp JJ, Boezeman JB, Adema GJ, Bulte JW, Scheenen TW, et al. Magnetic resonance tracking of dendritic cells in melanoma patients for monitoring of cellular therapy. *Nat Biotechnol* 2005;23: 1407–13.
13. Srinivas M, Heerschap A, Ahrens ET, Figdor CG, de Vries IJM. 19F MRI for quantitative in vivo cell tracking. *Trends Biotechnol* 2010;28:363–70.
14. Sengar RS, Spokauskiene L, Steed DP, Griffin P, Arbujas N, Chambers WH, Wiener EC. Magnetic resonance imaging-guided adoptive cellular immunotherapy of central nervous system tumors with a T1 contrast agent. *Magn Reson Med* 2009;62: 599–606.
15. Liu W, Frank JA. Detection and quantification of magnetically labeled cells by cellular MRI. *Eur J Radiol* 2009;70: 258–64.
16. Ahrens ET, Flores R, Xu H, Morel PA. In vivo imaging platform for tracking immunotherapeutic cells. *Nat Biotechnol* 2005;23:983–7.
17. Ruiz-Cabello J, Walczak P, Kedziorek DA, Chacko VP, Schmieder AH, Wickline SA, Lanza GM, Bulte JW. In vivo "hot spot" MR imaging of neural stem cells using fluorinated nanoparticles. *Magn Reson Med* 2008;60:1506–11.
18. Srinivas M, Morel PA, Ernst LA, Laidlaw DH, Ahrens ET. Fluorine-19 MRI for

visualization and quantification of cell migration in a diabetes model. *Magn Reson Med* 2007;58:725–34.
19. Srinivas M, Turner MS, Janjic JM, Morel PA, Laidlaw DH, Ahrens ET. In vivo cytometry of antigen-specific t cells using (19)F MRI. *Magn Reson Med* 2009;62: 747–53.
20. Boullart AC, Aarntzen EH, Verdijk P, Jacobs JF, Schuurhuis DH, Benitez-Ribas D, Schreibelt G, van de Rakt MW, Scharenborg NM, de Boer A, Kramer M, Figdor CG, et al. Maturation of monocyte-derived dendritic cells with Toll-like receptor 3 and 7/8 ligands combined with prostaglandin E2 results in high interleukin-12 production and cell migration. *Cancer Immunol Immunother* 2008;57:1589–97.
21. Helfer BM, Melson AD, Janjic JM, Gil RR, Kalinski P, de Vries J, Ahrens ET, Mailliard RB. Functional assessment of human dendritic cells labeledffor in vivo 19F magnetic resonance imaging cell tracking. Application of a novel 19F tracer agent for in vivo tracking of human dendritic cell vaccines. *Cytotherapy* 2010; 12:238–50.
22. Gudbjartsson H, Patz S. The Rician distribution of noisy MRI data. *Magn Reson Med* 1995;34: 910–4.
23. Janjic JM, Srinivas M, Kadayakkara DK, Ahrens ET. Self-delivering nanoemulsions for dual fluorine-19 MRI and fluorescence detection. *J Am Chem Soc* 2008;130: 2832–41.
24. Verdijk P, Scheenen TW, Lesterhuis WJ, Gambarota G, Veltien AA, Walczak P, Scharenborg NM, Bulte JW, Punt CJ, Heerschap A, Figdor CG, de Vries IJ. Sensitivity of magnetic resonance imaging of dendritic cells for in vivo tracking of cellular cancer vaccines. *Int J Cancer* 2007; 120:978–84.
25. Foster-Gareau P, Heyn C, Alejski A, Rutt BK. Imaging single mammalian cells with a 1.5 T clinical MRI scanner. *Magn Reson Med* 2003;49:968–71.
26. Heyn C, Bowen CV, Rutt BK, Foster PJ. Detection threshold of single SPIO-labeled cells with FIESTA. *Magn Reson Med* 2005; 53:312–20.
27. Hsiao JK, Tai MF, Chu HH, Chen ST, Li H, Lai DM, Hsieh ST, Wang JL, Liu HM. Magnetic nanoparticle labeling of mesenchymal stem cells without transfection agent: cellular behavior and capability of detection with clinical 1.5 T magnetic resonance at the single cell level. *Magn Reson Med* 2007;58: 717–24.
28. Cheung JS, Chow AM, Hui ES, Yang J, Tse HF, Wu EX. Cell number quantification of USPIO-labeled stem cells by MRI: an in vitro study. *Conf Proc IEEE Eng Med Biol Soc* 2006;1:476–9.
29. Liu W, Dahnke H, Jordan EK, Schaeffter T, Frank JA. In vivo MRI using positive-contrast techniques in detection of cells labeled with superparamagnetic iron oxide nanoparticles. *NMR Biomed* 2008;21: 242–50.
30. Seppenwoolde JH, Viergever MA, Bakker CJ. Passive tracking exploiting local signal conservation: the white marker phenomenon. *Magn Reson Med* 2003;50: 784–90.
31. Seppenwoolde JH, Vincken KL, Bakker CJ. White-marker imaging--separating magnetic susceptibility effects from partial volume effects. *Magn Reson Med* 2007;58: 605–9.
32. Rad AM, Arbab AS, Iskander AS, Jiang Q, Soltanian-Zadeh H. Quantification of superparamagnetic iron oxide (SPIO)-labeled cells using MRI. *J Magn Reson Imaging* 2007;26: 366–74.
33. De Vries IJ, Krooshoop DJ, Scharenborg NM, Lesterhuis WJ, Diepstra JH, Van Muijen GN, Strijk SP, Ruers TJ, Boerman OC, Oyen WJ, Adema GJ, Punt CJ, et al. Effective migration of antigen-pulsed dendritic cells to lymph nodes in melanoma patients is determined by their maturation state. *Cancer Res* 2003;63:12–17.
34. Dietrich O. Single-shot pulse sequences. In: Schoemberg S, Dietrich O, Reiser M, eds. Parallel imaging in clinical MR applicationsed. Berlin, Germany: Springer Berlin Heidelberg, 2007. 119–26.
35. Klomp D, van Laarhoven H, Scheenen T, Kamm Y, Heerschap A. Quantitative 19F MR spectroscopy at 3 T to detect heterogeneous capecitabine metabolism in human liver. *NMR Biomed* 2007;20: 485–92.
36. Li CW, Negendank WG, Padavic-Shaller KA, O'Dwyer PJ, Murphy-Boesch J, Brown TR. Quantitation of 5-fluorouracil catabolism in human liver in vivo by three-dimensional localized 19F magnetic resonance spectroscopy. *Clin Cancer Res* 1996;2:339–45.